

# EqDeepRx: Learning a Scalable MIMO Receiver

Mikko Honkala, Dani Korpi, Elias Raninen, and Janne M. J. Huttunen

*Nokia Bell Labs  
Espoo, Finland*

**Abstract**—While machine learning (ML)-based receiver algorithms have received a great deal of attention in the recent literature, they often suffer from poor scaling with increasing spatial multiplexing order and lack of explainability and generalization. This paper presents *EqDeepRx*, a practical deep-learning-aided multiple-input multiple-output (MIMO) receiver, which is built by augmenting linear receiver processing with carefully engineered ML blocks. At the core of the receiver model is a shared-weight *DetectorNN* that operates independently on each spatial stream or layer, enabling near-linear complexity scaling with respect to multiplexing order. To ensure better explainability and generalization, EqDeepRx retains conventional channel estimation and augments it with a lightweight *DenoiseNN* that learns frequency-domain smoothing. To reduce the dimensionality of the *DetectorNN* inputs, the receiver utilizes two linear equalizers in parallel: a linear minimum mean-square error (LMMSE) equalizer with interference-plus-noise covariance estimation and a regularized zero-forcing (RZF) equalizer. The parallel equalized streams are jointly consumed by the *DetectorNN*, after which a compact *DemapperNN* produces bit log-likelihood ratios for channel decoding. 5G/6G-compliant end-to-end simulations across multiple channel scenarios, pilot patterns, and inter-cell interference conditions show improved error rate and spectral efficiency over a conventional baseline, while maintaining low-complexity inference and support for different MIMO configurations without retraining.

## I. INTRODUCTION

Machine learning (ML)-based enhancements to wireless communication systems have received a great deal of attention in the recent years among the research community. Primary motivation for such research has been to obtain computationally feasible algorithms for very complex tasks, or obtain new types of data-driven algorithms, by emulating them with deep neural networks. Specifically in the physical layer, it has been shown that ML can bring significant gains in terms of spectral efficiency [1]–[3]. Practical challenges, such as memory and computational demands, however still remain and need to be adequately addressed before these techniques can be fully adopted in real networks.

In this paper, our focus is on ML-driven physical layer receiver processing. Previously, in [4], we proposed a deep learning orthogonal frequency-division multiplexing (OFDM) receiver DeepRx which was based on a convolutional neural network (CNN) architecture. In DeepRx, the CNN processes the received data for the whole transmission time interval (TTI) at once and outputs the log-likelihood ratios (LLRs) of the transmitted bits. The model was trained with simulated single-input multiple-output (SIMO) data and it reached high performance compared to a traditional receiver in simulated evaluations. In [5], we showed the benefits of incorporating *expert knowledge* via layers of operations building on traditional receiver signal processing in the architecture. This allowed the model to achieve competitive performance also with multiple-

input and multiple-output (MIMO) scenarios, with reasonable computational complexity.

Herein, we extend our previous deep learning based receiver DeepRx [4], [5] toward a structure that is tailored for meeting the high MIMO multiplexing order and throughput demands of practical receiver deployment in real-world networks in 6G and beyond. This is done by expanding on the idea of using expert knowledge together with deep learning. The improved receiver, which we call *EqDeepRx*, uses a novel architecture that combines parts of the conventional MIMO OFDM signal processing flow with neural network (NN) stages. A distinguishing feature of EqDeepRx is that it adopts a parallel equalizer (EQ) design that allows for reducing the computational complexity. As in [5], including EQs incorporates typical operations for equalization into the NN model (e.g. matrix inversions) that would be difficult to approximate with traditional NN structures without excessively high complexity. In this work, we utilize this EQ structure even further and design an neural network architecture that is invariant to the number of spatially multiplexed MIMO transmissions (i.e. MIMO layers). This is a desirable feature in practical deployments to allow flexible MIMO scheduling. Furthermore, we enable effective operation under strong inter-cell interference by utilizing an EQ specifically tailored for interference. Finally, we show that employing multiple parallel EQs can bring benefits both in performance and training stability.

The main contributions of this article are listed below.

- We propose a novel ML-based receiver, EqDeepRx, which combines conventional receiver processing with NN layers specifically designed to allow reasonable computational complexity. The defining characteristics of the EqDeepRx receiver model are: (i) introducing deep learning in the channel denoising and soft symbol detection phases, while relying on otherwise conventional receiver processing, (ii) taking advantage of two parallel equalizers, and (iii) scaling nearly linearly to support arbitrary number of MIMO layers, which also makes the receiver feasible for realistic systems.
- As one of EQs, we employ a *linear minimum mean square error* (LMMSE) equalizer with *interference-plus-noise covariance* (INCM) estimation allowing effective operation under strong inter-cell interference.
- To show that proposed EqDeepRx model achieves state-of-the-art performance, the model is evaluated across a wide range of channel conditions, both in terms of raw uncoded bit error rate (BER), as well as the block error rate (BLER) after channel decoding. The latter is also used to quantify the gain of the receiver in terms of spectral efficiency improvement. It is also demonstrated that the developed architecture can achieve good accuracy across different MIMO layer allocations without retraining.

- A comprehensive ablation study is performed, where the developed primary EqDeepRx architecture is compared to various alternatives in terms of ML processing and/or computational complexity. The absolute computational complexity of different EqDeepRx variants is also quantified and reported in terms of floating point operations (FLOPS).

The rest of this article is organized as follows. In Section II, we describe the basic system model, and also define the processing utilizing a LMMSE receiver. Then, in Section III, the proposed EqDeepRx model architecture is described in detail. After this, the simulation results, including the ablation study, are presented in Section IV, while Section V concludes the article.

### A. Related work

ML-based approaches have been successfully applied to many parts of the radio physical layer. Some of the more widely studied examples include channel estimation [6], [7], signal compression and detection [8], [9], and coding [10]. There is also a wide body of literature focusing on designing and training a complete receiver based on, at least partially, deep learning. The works in [11], [12] introduced two different approaches for learning a single-input single-output (SISO) receiver from data, using either a fully learned approach [11] or one where ML was combined with expert knowledge [12]. The aforementioned DeepRx ML receiver was proposed in [4], consisting of a fully convolutional ResNet model. All of these approaches were reported to provide performance gains over the conventional baselines in SISO transmission.

After these initial findings, the work has focused on scaling ML-based receiver approaches to cover a wider range of practical scenarios, while addressing the computational complexity. The problem of learning a MIMO detector was analyzed in [13], assuming perfect channel knowledge. In [5], DeepRx was extended for MIMO transmissions, where it was shown that in order to reach sufficient performance, the ML architecture should incorporate expert knowledge via additional processing blocks that resemble conventional receiver processing. Another ML-based receiver variant intended for MIMO OFDM systems was proposed in [14]. It builds on a combination of convolutional layers and graph neural networks (GNNs) to build an ML-based OFDM receiver that can operate with different numbers of MIMO streams. This model was purely relying on neural network layers, with no elements from conventional receivers included between the OFDM demodulator and channel decoder.

Use of GNNs within a receiver algorithm has also been investigated in [15]–[17]. The work in [15] implements a joint detector and decoder with a GNN, and demonstrates substantial performance gain over comparable baselines. In [16], GNN-based channel estimation for 5G is investigated, which is shown to slightly improve performance, while having significantly lower computational complexity. Another GNN-aided receiver approach is proposed in [17], where GNNs are utilized in the posterior estimation phase to compensate for approximation errors.

Most of the aforementioned works assume a linear system, where the ML-based algorithms are designed to outperform conventional receivers due to learning more accurate processing steps based on the training data distribution. However, significant research effort has also been focused on dealing with different hardware impairments by using deep learning. For instance, a DeepRx-type CNN receiver has been shown to be robust against power amplifier-induced nonlinear distortion when equipped with additional Fourier transforms [18]. The work in [19] demonstrated that ML-based demapper can be effective against such PA-induced distortion with discrete Fourier transform-spread OFDM (DFT-s-OFDM) waveforms.

An interesting longer-term line of research has focused on deep learning based end-to-end solutions that simultaneously optimize both the transmitter and the receiver. There are multiple proposals where the transmitter-receiver link is learned from data without necessarily any pre-specified modulation scheme [20]–[23]. The early work focused on a fully learned approach with learned waveforms [20], while the work has more recently focused on OFDM waveforms with some learned properties, such as constellation shape [21]–[23]. The main benefit of utilizing a learned constellation shape with a jointly learned ML receiver is that the system learns to communicate without any pilot signals, improving the spectral efficiency. More recently, the use of superimposed pilots has also been proposed as another approach for achieving similar spectral efficiency gain without necessarily having to modify the constellation shape [24]. However, despite the higher performance compared to utilizing only an ML-based receiver, implementing such end-to-end approaches in a practical radio network requires significant modifications to existing wireless standards, which can delay their implementation in practical systems.

This paper builds and extends on DeepRx, making it a realistic ML-based receiver meeting the practical demands of future cellular networks. This is accomplished via augmenting the architecture with carefully selected expert knowledge, which is in contrast with some of the other ML receivers in the literature (e.g., [14]). Moreover, we focus on evaluating the developed receiver under 5G/6G compliant OFDM waveforms, to ensure that the reported results reflect what is achievable in the 6G timeframe.

## II. SYSTEM MODEL

In this section we formulate the system model and outline the receiver processing steps that are used as a basis for the proposed EqDeepRx architecture. Figure 1 depicts the system model on a high level. Throughout the paper, we restrict our analysis to the uplink (UL) case, where one or several UEs transmit data to a base station (BS). However, most of the algorithms are applicable also to the downlink (DL) case.

Consider OFDM transmissions, where one or several UEs transmit a total of  $N_T$  spatial streams, also referred to as MIMO layers, to a base station with  $N_R$  RX antennas over the duration of one slot. We assume that the number of layers is equal to the number of transmit (TX) antennas. We denote the number of data carrying subcarriers by  $N_F$  and the number of OFDM symbols within a slot by  $N_S$  (typically  $N_S = 14$ ).

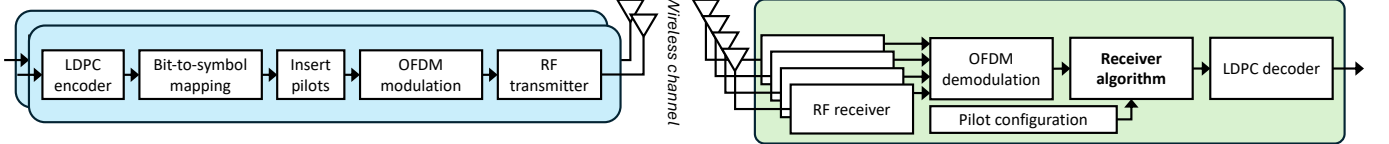


Fig. 1: Overall block diagram of the considered system. In this article, we consider different alternatives for the receiver algorithm part, including the conventional baseline as well as the proposed EqDeepRx ML receiver.

The baseband-equivalent model for the received signal  $\mathbf{y}_{ij} \in \mathbb{C}^{N_R \times 1}$  corresponding to the  $i$ th subcarrier in the  $j$ th OFDM symbol can be expressed as

$$\mathbf{y}_{ij} = \mathbf{H}_{ij} \mathbf{x}_{ij} + \mathbf{v}_{ij} + \mathbf{n}_{ij}, \quad (1)$$

where  $\mathbf{H}_{ij} \in \mathbb{C}^{N_R \times N_T}$  is a deterministic (non-random) channel matrix,  $\mathbf{x}_{ij} \in \mathbb{C}^{N_T \times 1}$  comprise the transmitted data signals corresponding to the MIMO layers,  $\mathbf{v}_{ij} \in \mathbb{C}^{N_R \times 1}$  constitutes the interfering signals, and  $\mathbf{n}_{ij} \in \mathbb{C}^{N_R \times 1}$  is the noise. We often use the notation  $\mathbf{d}_{ij} = \mathbf{v}_{ij} + \mathbf{n}_{ij}$  for the *interference-plus-noise* vectors. We assume that  $\mathbf{x}_{ij}$ ,  $\mathbf{v}_{ij}$ , and  $\mathbf{n}_{ij}$  are mutually independent and zero mean random vectors.

**Remark:** Note that the above frequency-domain model cannot express all physical time-domain channel phenomena such as inter-carrier interference (ICI) or inter-symbol interference (ISI). Hence, the interference term  $\mathbf{v}_{ij}$  is assumed to only include inter-cell interference consisting of overlapping transmissions of UEs in adjacent cells. However, we would like to highlight that while the signal model used for the receiver design does not accommodate ISI and ICI, the training data generation is carried out using a complete time-domain simulator. Therefore, both ISI and ICI effects are present in the simulations, and consequently the trained models can learn to mitigate these effects during training to the extent allowed by their model architectures and training procedures.

### A. Equalization

In EqDeepRx, we use two equalizers in parallel: the *regularized zero forcing* (RZF) equalizer and the LMMSE equalizer. For the signal model (1) (omitting the subscripts  $ij$ ), the RZF equalizer is defined as

$$\mathbf{W}_{\text{RZF}} = (\mathbf{H}^H \mathbf{H} + \alpha \mathbf{I})^{-1} \mathbf{H}^H, \quad (2)$$

where  $\alpha \mathbf{I}$  is a regularizing term. If  $\alpha = 0$ , we obtain the traditional zero-forcing (ZF) equalizer. In the simulations, we use the empirically determined value  $\alpha = 10^{-4}$ .

In order to perform the equalization in practice, we need estimates of the channel matrix for each resource element  $(i, j) \in \mathcal{D}$ , where  $\mathcal{D}$  denotes the set of data symbols. We provide detailed discussions regarding the channel estimation in Sec. II-B. Given the channel estimates  $\widehat{\mathbf{H}}_{ij}$ , we plug them in to (2) to obtain  $\widehat{\mathbf{W}}_{ij, \text{RZF}}$ . Since we desire unit-gain symbols, we further scale the equalizer by the inverse of  $\mathbf{D}_{ij, \text{RZF}} = \text{diag}(\widehat{\mathbf{W}}_{ij, \text{RZF}} \widehat{\mathbf{H}}_{ij})$ , yielding the equalized symbols

$$\widehat{\mathbf{x}}_{ij, \text{RZF}} = \mathbf{D}_{ij, \text{RZF}}^{-1} \widehat{\mathbf{W}}_{ij, \text{RZF}} \mathbf{y}_{ij}, \quad (i, j) \in \mathcal{D}. \quad (3)$$

As for the LMMSE equalizer,  $\mathbf{W}_{\text{LMMSE}}$ , it is defined as the linear filter that minimizes the mean squared error (MSE)

between the estimated and transmitted symbols. For the signal model (1) (omitting the subscripts  $ij$ ), it is given by

$$\mathbf{W}_{\text{LMMSE}} = \arg \min_{\mathbf{W} \in \mathbb{C}^{N_R \times N_T}} \mathbb{E}[\|\mathbf{x} - \mathbf{W}\mathbf{y}\|^2] = \mathbf{R}_{\mathbf{xy}} \mathbf{R}_{\mathbf{y}}^{-1}, \quad (4)$$

where  $\mathbf{R}_{\mathbf{y}} = \mathbb{E}[\mathbf{y}\mathbf{y}^H] = \mathbf{H}\mathbf{R}_{\mathbf{x}}\mathbf{H}^H + \mathbf{R}$ ,  $\mathbf{R}_{\mathbf{xy}} = \mathbb{E}[\mathbf{xy}^H] = \mathbf{R}_{\mathbf{x}}\mathbf{H}^H$ ,  $\mathbf{R}_{\mathbf{x}} = \mathbb{E}[\mathbf{x}\mathbf{x}^H]$ , and

$$\mathbf{R} = \mathbb{E}[\mathbf{dd}^H] = \mathbb{E}[(\mathbf{v} + \mathbf{n})(\mathbf{v} + \mathbf{n})^H] \quad (5)$$

is the INCM. As the constellation must be known both by the transmitter and the receiver, we may assume  $\mathbf{R}_{\mathbf{x}} = \mathbf{I}$ , and the equalizer simplifies to

$$\mathbf{W}_{\text{LMMSE}} = \mathbf{H}^H (\mathbf{H}\mathbf{H}^H + \mathbf{R})^{-1}. \quad (6)$$

In a practical implementation, in addition to the estimated channel matrix, we also need to estimate the INCM. However, instead of obtaining an estimate for each resource element, the INCM  $\mathbf{R}$  is estimated over each *interference coherence bandwidth* defined as the interval of subcarriers for which the interference statistics may be assumed to remain approximately constant. We provide a detailed discussion regarding the estimation of the INCM in Sec. II-C.

Assuming we have channel estimates  $\widehat{\mathbf{H}}_{ij}$  and an estimate  $\widehat{\mathbf{R}}$  of the INCM, we may plug in the estimates in (6) to obtain  $\widehat{\mathbf{W}}_{ij, \text{LMMSE}}$ . In order to obtain unit-gain symbols, as before we further scale the equalizer by the inverse of  $\mathbf{D}_{ij} = \text{diag}(\widehat{\mathbf{W}}_{ij, \text{LMMSE}} \widehat{\mathbf{H}}_{ij})$ , yielding the estimated symbols

$$\widehat{\mathbf{x}}_{ij, \text{LMMSE}} = \mathbf{D}_{ij, \text{LMMSE}}^{-1} \widehat{\mathbf{W}}_{ij, \text{LMMSE}} \mathbf{y}_{ij}, \quad (i, j) \in \mathcal{B}, \quad (7)$$

where  $\mathcal{B}$  denotes the set of indices corresponding to REs carrying data symbols in an interference coherence bandwidth.

**Remark:** the LMMSE equalizer can also be expressed in the form  $\mathbf{W}_{\text{LMMSE}} = (\mathbf{H}^H \mathbf{R}^{-1} \mathbf{H} + \mathbf{I})^{-1} \mathbf{H}^H \mathbf{R}^{-1}$ . Since  $N_T \ll N_R$  and the inverse of  $\mathbf{R}$  need to be calculated only once for each interference coherence bandwidth, this form is usually less computationally expensive. Also note, that given the alternative formulation of the LMMSE and the fact that we assumed  $\mathbf{R}_{\mathbf{x}} = \mathbf{I}$ , the only remaining difference between the RZF and the LMMSE is that  $\mathbf{R}$  is replaced with  $\alpha \mathbf{I}$ .

### B. Channel estimation

To perform equalization, we must first estimate the channel matrices  $\mathbf{H}_{ij}$  for all subcarriers  $i = 1, \dots, N_F$  and all OFDM symbols  $j = 1, \dots, N_S$ . To this end, pilot information or demodulation reference signals (DMRSs) that are *a priori* known at the receiver constitute a portion of the transmitted data. The pilot information need to be multiplexed and processed so that decent estimates can be obtained for each layer (i.e., each column of the channel matrix). Regardless of the specific

type of multiplexing, the receiver first calculates rank one raw channel estimates using

$$\hat{\mathbf{H}}_{ij,\text{raw}} = \frac{1}{\|\mathbf{x}_{ij}\|_2^2} \mathbf{y}_{ij} \mathbf{x}_{ij}^H, \quad (i, j) \in \mathcal{P}, \quad (8)$$

where  $\mathcal{P} = \{(i, j) : \mathbf{x}_{ij} \text{ contains pilot information}\}$  and  $\|\cdot\|_2$  denotes the Euclidean norm. We assume pilot sequences that are orthogonal in time and frequency (i.e., no code domain multiplexing). Hence, a single pilot symbol in a specific RE is used to estimate a specific layer (column of the channel matrix) at that specific  $(i, j) \in \mathcal{P}$ , meaning that each pilot symbol  $\mathbf{x}_{ij}$  only has one non-zero element and consequently the individual raw channel matrix estimates contain only one non-zero row. In order to obtain the final channel matrix estimates denoted by  $\hat{\mathbf{H}}_{ij}$  for all resource elements, we utilize linear interpolation followed by smoothing, or denoising, by a static frequency-domain filter.

### C. Interference-plus-noise covariance matrix (INCM) estimation

The INCM  $\hat{\mathbf{R}}$  is computed for each interference coherence bandwidth, which is an interval of subcarriers for which we may assume that the interference statistics remain approximately static. We use a interference coherence bandwidth corresponding to two PRBs equaling 24 subcarriers.

Let  $\mathcal{B}$  denote an index set of resource elements corresponding to a particular interference coherence bandwidth. The INCM corresponding to  $\mathcal{B}$  is computed from the interference-plus-noise vectors estimated from the pilot symbols in  $\mathcal{B}$ . Hence, the interference-plus-noise vectors are estimated via

$$\hat{\mathbf{d}}_{ij} = \mathbf{y}_{ij} - \hat{\mathbf{H}}_{ij} \mathbf{x}_{ij}, \quad (i, j) \in \mathcal{P} \cap \mathcal{B}.$$

An initial estimate of the covariance  $\mathbf{R}$  is obtained by computing the sample covariance matrix

$$\hat{\mathbf{S}} = \frac{1}{P} \sum_{i, j \in \mathcal{P} \cap \mathcal{B}} \hat{\mathbf{d}}_{ij} \hat{\mathbf{d}}_{ij}^H,$$

where  $P = |\mathcal{P} \cap \mathcal{B}|$ , i.e., the number of pilot symbols in  $\mathcal{B}$ . The accuracy of the estimator is further improved using linear shrinkage estimation defined by

$$\hat{\mathbf{S}}(\rho) = (1 - \rho) \hat{\mathbf{S}} + \rho [\text{tr}(\hat{\mathbf{S}})/N_R] \mathbf{I}, \quad \rho \in [0, 1]. \quad (9)$$

The shrinkage parameter  $\rho$  is select using the complex-valued version [25] of the oracle approximating shrinkage (OAS) method [26], which approximates the MMSE minimizing shrinkage parameter under the assumption of complex Gaussian interference and noise. Note that, in the simulations as well as in real settings, the interference is not exactly complex Gaussian, but the approximation works well enough.

### D. Demapping and Decoding

The final step in the physical layer receiver chain is to perform demapping, in which posterior probabilities of sent bits (soft bits) are calculated based on the symbol estimates

$\hat{x}_{ij}$ . The demapping is typically carried out by calculating the log-likelihood ratios (LLRs),

$$L_{ijkl} = \log \left( \frac{\Pr(c_l = 0 | \hat{x}_{ijk})}{\Pr(c_l = 1 | \hat{x}_{ijk})} \right), \quad l = 0, \dots, B - 1 \quad (10)$$

where  $\Pr(c_l = 0/1 | \hat{x}_{ijk})$  is the conditional probability that the transmitted  $l$ th bit on  $i$ th subcarrier,  $j$ th OFDM symbol, and  $k$ th MIMO layer is 0/1 given the observed symbol  $\hat{x}_{ijk}$ , and  $B$  is the number of bits per symbol. For further details about the demapper, please refer to [4].

After demapping, the obtained LLRs are fed to the the low-density parity-check (LDPC) decoder to compute final information bits from the estimated LLRs. In this work, we utilize 5G-compliant LDPC channel coding [27], but we omit a more detailed description for brevity.

## III. EQDEEPRX

The original DeepRx architecture [4] demonstrated significant gains in SIMO scenarios by processing the entire TTI's received data  $\mathbf{y}$  and raw channel estimate  $\hat{\mathbf{H}}$  with a ResNet-based CNN to produce all LLRs jointly. We attributed these gains to the network's learned ability to exploit known symbol constellations and track both time- and frequency-selective fading.

When extending DeepRx to MIMO in [5], we first explored two variants: (i) a ResNet augmented with a maximum ratio combining (MRC) equalizer, and (ii) a fully-learned multiplicative transformation embedded within the network. Although both architectures improved upon practical baselines, they proved suboptimal in practice—either incurring excessive filter counts and computational cost or failing to deal with inter-cell interference. We attributed this to the fact that the neural network needed to learn and approximate operations similar to, for example, the matrix inversion to deal with inter-cell and inter-layer interference.

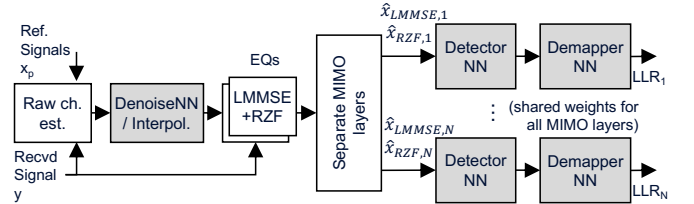


Fig. 2: EqDeepRx high-level architecture. MIMO layers are handled in parallel separately after the EQs, allowing for efficient inference and layer count generalization. Blocks with gray background contain trainable parameters.

These findings motivate our hybrid **EqDeepRx** design shown in Fig. 2. EqDeepRx unites proven signal-processing components with a compact, per-MIMO-layer neural detector. Our key design principles are:

- **Hybrid channel estimation:** We retain DMRS-based raw channel estimation (Eq. (8)), followed by linear interpolation. We replace a traditional frequency-domain smoothing by a neural network *DenoiseNN* which processes per-antenna data streams and can learn to properly denoise

raw antenna signals. This mixture of deterministic and learned processing improves channel estimation quality while having reasonable FLOPs.

- **Parallel equalization:** We apply both RZF and LMMSE equalizers in parallel to the denoised, interpolated channel estimate. This dual-branch approach yields superior interference suppression and noise-whitening, and by offloading equalization to classical algorithms, avoids inflating the neural network's size.
- **Per-MIMO-layer DetectorNN:** After equalization, MIMO layers are assumed to be separated. A lightweight residual network—built from depthwise-separable 2D convolutions (alternating  $1 \times N$  and  $N \times 1$  kernels with subsampling)—then processes each layer independently. By exploiting known constellation structure and tracking time–frequency variations, this DetectorNN delivers the bulk of the performance gains while scaling near-linearly in the number of layers.

As shown in Fig. 2, EqDeepRx takes as input the full-TTI received signal  $\mathbf{y}$  and DMRS pilots, computes a raw channel estimate (Sec. II-B), applies parallel RZF/LMMSE equalizers (Sec. II-A), then splits the per-layer outputs into the neural networks to produce final LLRs. Details are given in the following.

#### A. Channel estimation and DenoiseNN

In order to deal with varying channel and SNR situations in channel smoothing phase, we replace the conventional frequency-domain smoothing filter with a learned *DenoiseNN*. As summarized in Table I, DenoiseNN operates *only at pilot positions* and is applied *independently for each RX-TX antenna pair*  $(r, t)$ , i.e., for each complex pilot grid  $\hat{H}_{\text{raw}}^{(r,t)} \in \mathbb{C}^{F_P \times S_P}$  extracted from  $\hat{\mathbf{H}}_{\text{raw}}$ . Note that  $F_P$  and  $S_P$  denote the amount of pilot symbols along the subcarrier and OFDM symbol axes, respectively.

For each pair  $(r, t)$ , we first split complex values into two real channels (real/imag), yielding a tensor in  $\mathbb{R}^{F_P \times S_P \times 2}$ . This is processed by lightweight ResNet blocks applying down and upsampling for low-complexity smoothing / denoising operation (see III-C for details). The blocks applies 1D convolutions in the frequency direction while preserving per-symbol structure in time.

To allow the denoiser to access all pilot symbols, we insert a lightweight *symbol/time mixer* implemented as a shared *pointwise* ( $1 \times 1$ ) *convolution* after each ResNet block. Concretely, for each pilot subcarrier, we reshape the features so that the  $S_P$  pilot symbols are stacked into the channel dimension (for a small subset  $C_s$  of channels), apply a  $1 \times 1$  conv to linearly mix these stacked features *independently for each subcarrier* (i.e., with weights shared over frequency), and then reshape back. The remaining channels bypass the mixer, and a residual connection is used. See Table I for detailed list of operations.

After denoising, we obtain the full-grid channel estimate  $\hat{\mathbf{H}} \in \mathbb{C}^{F \times S \times N_R \times N_T}$  by the same linear interpolation step as in the baseline, i.e., interpolating from the pilot grid  $(F_P, S_P)$  to the full resource-element grid  $(F, S)$ . In summary, DenoiseNN

learns the pilot-domain smoothing that would otherwise be implemented by a fixed low-pass filter, while keeping the remainder of the channel-estimation pipeline conventional and lightweight.

#### B. Per-MIMO-Layer DetectorNN

Equalization (Sec. II-A) with both LMMSE and RZF equalizers produces two complex tensors

$$\hat{\mathbf{X}}_{\text{LMMSE}}, \hat{\mathbf{X}}_{\text{RZF}} \in \mathbb{C}^{N_F \times N_S \times N_T}.$$

For each MIMO layer  $t$ , we extract the  $t$ th slice of both tensors, concatenate along the channel axis, and split real/imaginary parts into separate channels to form

$$\tilde{\mathbf{X}}_t \in \mathbb{R}^{N_F \times N_S \times 4},$$

which is the symbol input into the DetectorNN branch for layer  $t$ .

In addition, we provide DetectorNN with explicit position information along the frequency and OFDM-symbol axes by concatenating two fixed coordinate maps (similar in spirit to [28]). Specifically, we form a normalized subcarrier-index map and a normalized symbol-index map,  $\mathbf{M}_F, \mathbf{M}_S \in \mathbb{R}^{N_F \times N_S \times 1}$ , with entries  $[\mathbf{M}_F]_{f,s} = 2 \frac{f}{N_F-1} - 1$  and  $[\mathbf{M}_S]_{f,s} = 2 \frac{s}{N_S-1} - 1$ , broadcast over the other dimension. Concatenating these maps to the real/imaginary LMMSE/RZF channels yields the final DetectorNN input

$$\tilde{\mathbf{X}}_t^{\text{pos}} = \text{concat}(\tilde{\mathbf{X}}_t, \mathbf{M}_F, \mathbf{M}_S) \in \mathbb{R}^{N_F \times N_S \times 6},$$

allowing the convolutional filters to learn frequency-/time-position-dependent processing when beneficial (for example DMRS symbol positions in time and input borders).

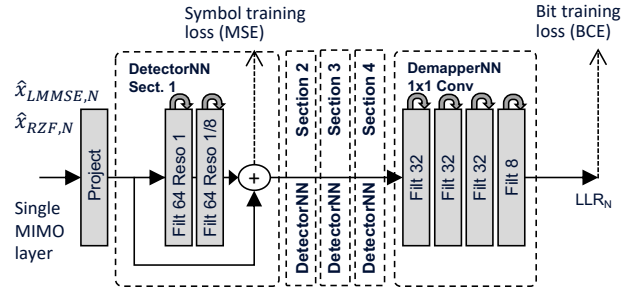


Fig. 3: Architecture of the DetectorNN and DemapperNN. This part of the model handles each MIMO layer separately in parallel.

DetectorNN, depicted in Fig. 3, processes each MIMO layer independently with shared weights. For layer  $t$ , the real-valued input  $\tilde{\mathbf{X}}_t \in \mathbb{R}^{N_F \times N_S \times 4}$  is first projected via a  $1 \times 1$  2D convolution to produce

$$\tilde{\mathbf{X}}_t^{(0)} \in \mathbb{R}^{N_F \times N_S \times C},$$

where  $C$  is the network's channel count. While this projection could be avoided via skip-connection projections, it makes the setup easier and does not affect link performance. The network then consists of  $S$  sections (typically  $S = 4$ ), each comprising

two residual blocks described in Sec. III-C at full ( $N = 1$ ) and one-eighth resolution ( $N = 8$ ).

Each section  $s$  also applies a section-level shortcut: if  $\tilde{\mathbf{X}}_t^{(s-1)}$  is the input to the section and  $\mathbf{Z}_t^{(s)}$  is the updated tensor after applying the residual blocks, the section-level output is then  $\tilde{\mathbf{X}}_t^{(s)} = \tilde{\mathbf{X}}_t^{(s-1)} + \mathbf{Z}_t^{(s)}$  (see Figure 3).

### C. Subsampled Residual Blocks

Inspired by [29], we reduce the computational complexity of the residual networks by subsampling some of the residual blocks, while keeping the residual path in full resolution. In addition, we separate 2D convolutions into two consecutive 1D convolutions, similar to [30].

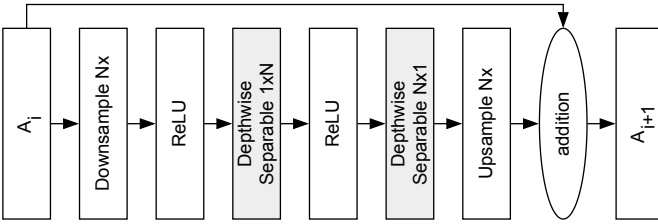


Fig. 4: The subsampling residual block for DetectorNN. DenoiseNN has similar structure, but both convolutions have  $N \times 1$  kernels for frequency-only operation.

Figure 4 depicts the subsampling residual block used in DetectorNN and DenoiseNN. Let  $D$  denote the  $N:1$  downsampling operator and  $U$  its inverse. The block implements

$$A_{i+1} = A_i + (U \circ f \circ D)(A_i), \quad (11)$$

with

$$f = DW_{13 \times 1} \circ \text{ReLU} \circ DW_{1 \times 13} \circ \text{ReLU} \quad (12)$$

using two depthwise-separable 2D convolutions with asymmetric  $1 \times 13$  and  $13 \times 1$  kernels. This design preserves detailed information from each RE via the residual connection, while keeping FLOPs low. We use a simple nearest-neighbour subsampling strategy both in down and upsampling. Note that when the input and output channel counts differ, we use the standard approach of projecting the skip (residual) branch with a  $1 \times 1$  (pointwise) convolution.

### D. DemapperNN

DemapperNN (see Figure 3) is a learned demapper that processes each MIMO layer and resource element independently. It begins with the real-valued frequency-time feature map  $\tilde{\mathbf{X}}^{(S)}$  produced by DetectorNN and then applies four standard ResNet-style residual blocks—each using two  $1 \times 1$  convolutions and ReLU activations—into bit-wise LLRs. Note that  $1 \times 1$  convolution corresponds to a fully connected layer applied to each RE independently (and via the global architecture, to each MIMO layer independently).

Finally, the output of the fourth and final residual block, denoted by  $D^{(4)}$ , already has channel dimension  $B$ , i.e., one channel per bit. Therefore, no additional output projection

is required, and the per-bit log-likelihood ratios are read out directly as

$$\text{LLR}_b = [D^{(4)}]_b, \quad b = 1, \dots, B.$$

Note that, similar to [4], we use  $B = 8$  to support a maximum modulation order of 256-QAM and extract only the required number of LLRs when using lower modulation orders.

### E. Training EqDeepRx

Inspired by [4], [21], training of EqDeepRx is carried out by optimizing the weighted cross-entropy loss extended with a symbol loss. We define the total loss for the  $q$ th sample as follows:

$$L_q(\theta) = \log_2(1 + \text{snr}_q) \left( \underbrace{\text{CE}_q(\theta) + \lambda \sum_{s=1}^S \|\tilde{\mathbf{X}}_q^{(s)}(\theta) - \mathbf{X}_q\|_2^2}_{L_{\text{bit},q}} \right) \underbrace{\sum_{s=1}^S \|\tilde{\mathbf{X}}_q^{(s)}(\theta) - \mathbf{X}_q\|_2^2}_{L_{\text{sym},q}} \quad (13)$$

where  $\theta$  denotes the set of trainable parameters,  $\text{CE}_q(\cdot)$  denotes binary cross entropy,  $\text{snr}_q$  is the linear signal-to-noise ratio (SNR) of the sample, and  $\lambda$  is a tunable parameter. In the training, we used an experimentally chosen  $\lambda = 10^{-4}$ . For the symbol loss,  $\mathbf{X}_q$  and  $\tilde{\mathbf{X}}_q^{(s)}$  are the ground truth and the predicted symbol after each state  $s$ , respectively. The latter is chosen to be the first two channels of the DetectorNN output (after the residual sum) that are reinterpreted as the real and imaginary parts (the remaining channels carrying auxiliary features).

To improve training stability, several approaches such as batch normalization layers can be used. In this work, we chose to regularize the per-channel batch-spatial mean and variance toward fixed targets,

$$\mathcal{L}_{\text{mVCL}} = \alpha \frac{\|\hat{\mu} - \mu_*\|_2^2 + \|\hat{v} - \sigma_*^2\|_2^2}{C},$$

where  $\hat{\mu}, \hat{v}$  are per-channel mean/variance (over batch and spatial dimensions), with  $\mu_* = 0$ ,  $\sigma_*^2 = 1$ , and  $\alpha = 10^{-5}$  and  $C$  the number of channels in a layer. This is a simplified variant of VCL [31]. However, we have experimentally noticed that our results are not specific to this specific choice and similar results can be reached with normalizations.

## IV. SIMULATION RESULTS

The training and performance evaluations of the proposed EqDeepRx ML receiver are carried out using Sionna open source library [32]. In particular, we have simulated the system depicted in Fig. 1 to first produce training data in an online fashion, after which we have validated the models under the chosen scenarios. Note that the online training data generation prevents overfitting by generating novel training data samples for each training batch. The detailed configuration of EqDeepRx is described in Table I, which represents the primary model architecture and is used unless stated otherwise. For training, we used a batch size of 112, initial learning rate of 0.004 for the LAMB optimizer, linear learning rate decay to zero, and  $\sim 70$ k iterations (training consisted of  $\sim 8$ M samples). Table II

TABLE I: Details of DenoiseNN, DetectorNN and DemapNN with default configuration. DenoiseNN operates per antenna pair, while DetectorNN and DemapperNN operate per MIMO layer. Note that depth refers to the number of ResNet blocks.

Section	Layer	Description	Output shape	Filters	Depth	Subsample	Kernel sizes
Channel est.	Input (H at pilots)	Channel matrix at pilot pos.	$(F_P, S_P, N_R, N_T)$	-	-	-	-
	ForEachAntennapair	Each antenna pair separately over $N_R, N_T$	$(F_P, S_P, 1)$	-	-	-	-
	Complex→Real	Convert complex to two real channels	$(F_P, S_P, 2)$	-	-	-	-
	DenoiseNN	ResNet stack w/ time mixing	$(F_P, S_P, 2)$	[64, 64, 64, 2]	4	1,4,2,1	$13 \times 1$
	Real→Complex	Convert real back to complex	$(F_P, S_P, 1)$	-	-	-	-
	CombineAntennas	Reshape per-pair outputs back to $(N_R, N_T)$	$(F_P, S_P, N_R, N_T)$	-	-	-	-
	Interpolate pilots to full	Interpolate from $(F_P, S_P)$ to full grid $(F, S)$	$(F, S, N_R, N_T)$	-	-	-	-
Equalizers	LMMSE   RZF	Inputs: denoised $H$ $(F, S, N_R, N_T)$ and $Y$ $(F, S, N_R)$ ; stack $\hat{X}$ across $E=2$	$(F, S, N_T, E=2)$	-	-	-	-
DetectorNN	ForEachLayer (over $N_T$ )	Process each MIMO layer separately $N_T$	$(F, S, 2)$	-	-	-	-
	Complex→Real	Convert complex streams to real	$(F, S, 4)$	-	-	-	-
	ConcatPosMaps	Concat frequency and symbol coordinate maps	$(F, S, 6)$	-	-	-	-
	Project	Linear 1x1 conv projection	$(F, S, 64)$	-	-	-	-
	Section 1/4	ResNet stack and section shortcut	$(F, S, 64)$	[64, 64]	2	1,8	$13 \times 1, 1 \times 13$
	Section 2/4	ResNet stack and section shortcut	$(F, S, 64)$	[64, 64]	2	1,8	$13 \times 1, 1 \times 13$
	Section 3/4	ResNet stack and section shortcut	$(F, S, 64)$	[64, 64]	2	1,8	$13 \times 1, 1 \times 13$
	Section 4/4	ResNet stack and section shortcut	$(F, S, 64)$	[64, 64]	2	1,8	$13 \times 1, 1 \times 13$
DemapperNN	Output (per-layer symbols)	Refined per-layer symbol estimates	$(F, S, 64)$	-	-	-	-
	ResNet stack	Output LLR estimates per bit for single layer	$(F, S, B)$	[32, 32, 32, B]	4	1,1,1,1	$1 \times 1$
Output	CombineMIMOLayers	Stack/gather per-layer LLRs back along $N_T$	$(F, S, N_T, B)$	-	-	-	-

Dimensions:  $F = 192$  (subcarriers),  $S = 14$  (OFDM symbols),  $N_R = 16$  (RX antennas),  $N_T = 4$  (MIMO layers),  $B = 8$  (bits),  $E = 2$  Eqs. Batch dim. omitted for clarity.

TABLE II: Key simulation parameters of the numerical experiments.  $\mathcal{U}$  denotes uniform distribution.

Parameter	Training	Validation
Channel model	UMa	UMa, CDL-C, CDL-D
Waveform	OFDM, 30 kHz SCS	
No. of subcarriers	192	
No. of OFDM symbols per slot	14	
No. of RX antennas	16	
No. of MIMO layers	2–4	
No. of UE TX antennas	1	
SNR	$\mathcal{U}(0 \text{ dB}, 45 \text{ dB})$	Varied
INR	Lognormal (10 dB, 5 dB)	
No. of interfering UEs	1	
UE speed	$\mathcal{U}(0 \text{ m/s}, 35 \text{ m/s})$	Varied
Delay spread	UMa	10–1100 ns
Modulation order		64-QAM
Code rate	N/A	MCS Table 2
DMRS configuration	1 or 2 OFDM pilot symbols per slot	

collects the key training and validation parameters, used in the forthcoming results unless stated otherwise.

The EqDeepRx model was trained using the Urban Macro (UMa) channel model, as defined in 3GPP TR 38.901 [33], using a wide range of SNRs and UE speeds. This channel model was adopted for training due to its randomized nature, for example, in terms of channel frequency selectivity and angular characteristics. In the performance validation results, also CDL-C and CDL-D channel models are used, in addition to UMa. Moreover, the model is trained without any error correction code, but when validating, low-density parity check (LDPC) encoding and decoding is used, in accordance with 5G specifications. In this work, we focus on 64-QAM which means that only those modulation and coding schemes (MCSs) are used. With the adopted MCS Table 2 [34], this corresponds to MCS indices 11–19. These MCSs cover code rates from 0.46 to 0.85. The used DMRS configuration is fully orthogonal across a maximum of four UEs. This is done by allocating the pilot symbols of each MIMO layer on every fourth subcarrier

within a physical resource block (PRB), with staggered offsets. A similar allocation is used on all DMRS-carrying OFDM symbols.

The interference is modeled by generating a transmit signal from one interfering UE with a random timing offset. The signal of the interfering UE experiences an independently randomized propagation channel, and the interfering power is determined by a log-normally distributed interference-to-noise ratio (INR). This ratio determines what is the relative power of the interfering signal with respect to the receiver noise power. Note that in the forthcoming figures, the SINR is calculated based on the combined effect of the random interference-plus-noise power realizations for each slot. The figures are generated by dividing the validation samples into a predefined number of bins based on the SINR realizations and averaging the ensuing quantities within these bins. For each validation, we used 32k samples. Lastly, it should be noted that, for all main results of EqDeepRx throughout this paper, we use the same trained model. The same single model also handles both of the utilized demodulation reference signal (DMRS) configurations.

#### A. Bit and Block Error Rate

Let us first analyze the EqDeepRx performance in terms of bit error rate (BER) and block error rate (BLER). The former is calculated directly from the model output, using the encoded transmit bit sequence as the ground truth values. The latter is determined based on the LDPC output, where a block is considered to have been correctly received if the decoded bit sequence matches with the transmitted information bits. The amount of information bits is aligned between the two DMRS configurations by using a larger MCS when there are 2 DMRS symbols. In the following results, we use MCSs 11 and 12 for slots with 1 DMRS and 2 DMRS, respectively. Since each slot contains 14 OFDM symbols in total, this means that the ensuing data rates are nearly identical (the slots with 1 DMRS carry

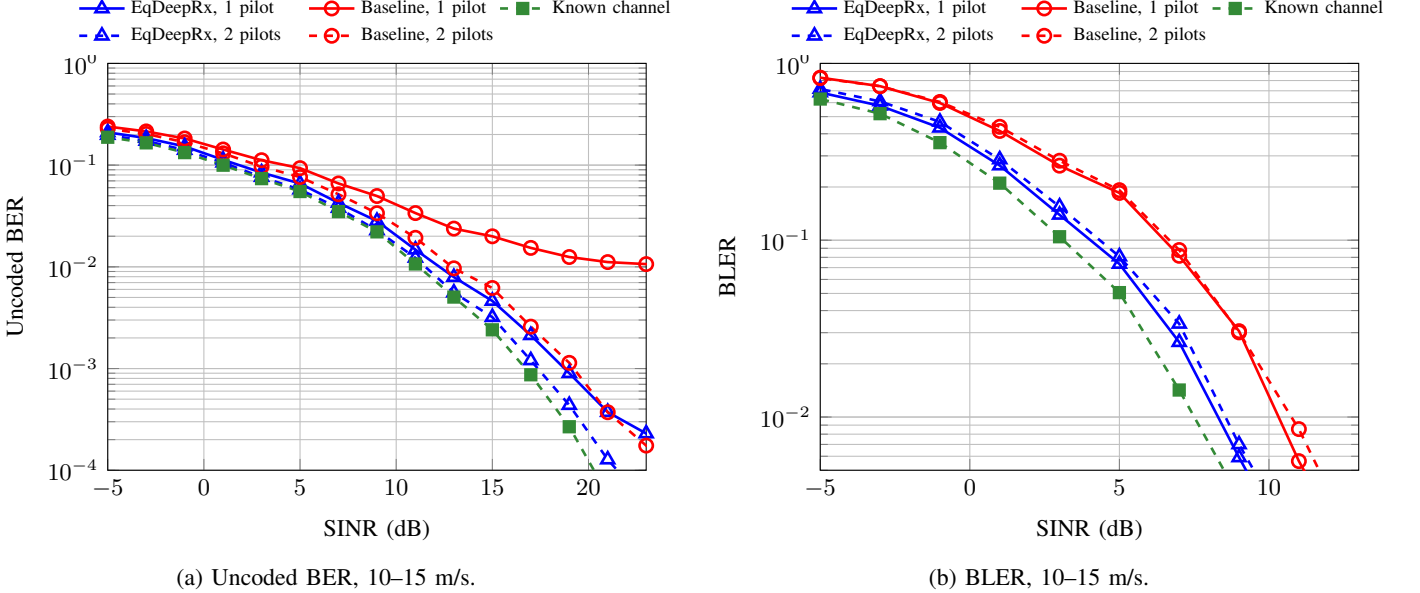


Fig. 5: Simulated (a) uncoded BER and (b) BLER with CDL-C, under speed of 10–15 m/s. Data rate matched MCSs.

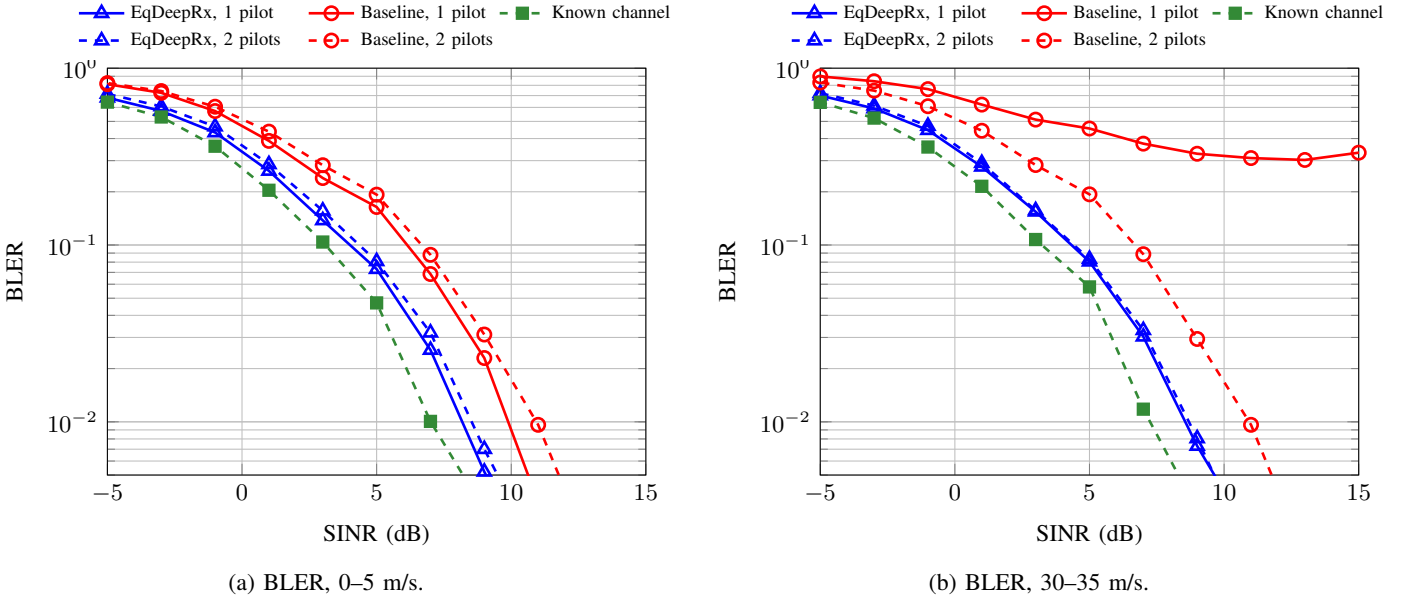


Fig. 6: Simulated BLER with CDL-C, under speeds of (a) 0–5 m/s and (b) 30–35 m/s. Data rate matched MCSs.

2.4% less information bits). With this, the different DMRS configurations can be compared within the same BLER plot, since the lower MCS of the 1 DMRS slots results in higher redundancy and better decoding performance, at the cost of a less accurate channel estimate.

For brevity, the EqDeepRx performance is shown for different UE speeds only with the CDL-C channel, whereas the CDL-D and UMa validations are only shown for a single speed range. This is because the relevant conclusions are the same across all the tested channel models. The baseline receiver is utilizing classical signal processing with LS channel estimation and LMMSE equalization, as described in Section II. In addition, the BER and BLER of a baseline with full channel knowledge is also shown. Note that in the forthcoming performance results this baseline is always using the smaller of the two MCS indices.

First, Figs. 5 and 6 show the performance of the different solutions with CDL-C channel model, across three different speed ranges. The uncoded BER before channel decoding is shown for the UE speed range of 10–15 m/s in Fig. 5, while only BLER is shown for the other speed ranges in Fig. 6, for brevity. It can be observed that with UE speed of 10–15 m/s EqDeepRx outperforms the baseline both in terms of uncoded BER and BLER. The former can be considered a measure of the accuracy of the hard bit decisions at the model output, while the latter factors in also the effect of the LLR magnitudes as well as the reduced overhead of the 1 DMRS configuration. With the chosen rather low MCS levels, EqDeepRx achieves nearly similar BLER performance with the 1 pilot and 2 pilot configurations, even though the uncoded BER degrades at the very highest UE speeds. When assuming a typical BLER value of 10%, the gain provided by EqDeepRx is in the order of 2

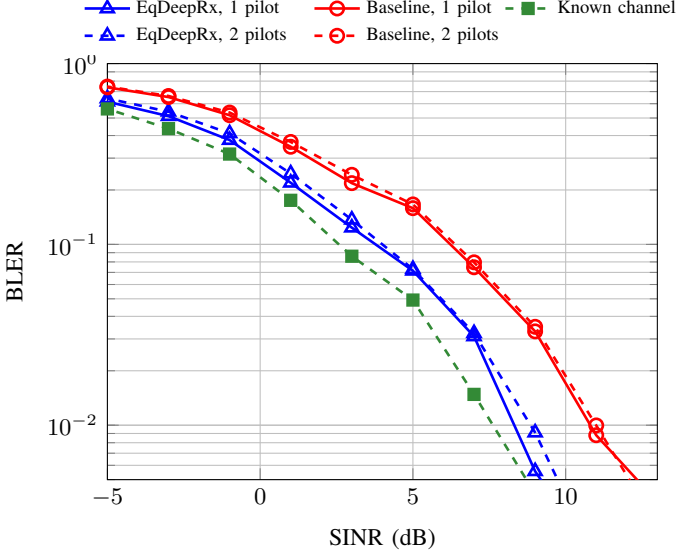


Fig. 7: BLER with CDL-C, UE speed of 10–15 m/s, and RMS delay spread of 10–100 ns.

dB in this scenario.

Similar performance gains are observed with the low and high speed scenarios in Fig. 6. With very low mobility, both the EqDeepRx and the baseline achieve the best performance with 1 DMRS, while in the high velocity case the baseline requires 2 DMRSs to achieve the typical operating point of 10% BLER. EqDeepRx achieves identical BLER both with 1 and 2 DMRSs, indicating that it is not very susceptible to channel aging even with high UE speeds. In this scenario, the somewhat worse LLR quality is compensated by the higher redundancy of the lower MCS index.

To obtain further insight into how the EqDeepRx model performs under different channel conditions, Figs. 7, 8 and 9 show the BLER validation results for three additional channel scenarios: CDL-C and CDL-D with a maximum root mean square (RMS) delay spread of 100 ns, and UMa channel model. Each scenario is simulated with UE speeds of 10–15 m/s.

Investigating first the CDL-C simulation results with the reduced delay spread in Fig. 7, we can observe good alignment with the higher delay spread scenario in Fig. 5. This indicates that the performance gain provided by EqDeepRx is not restricted to only very frequency selective channels.

The CDL-D channel model used in Fig. 8 represents a line-of-sight scenario with a maximum RMS delay spread of 100 ns. This scenario seems to favor the 1 DMRS case somewhat more since both the EqDeepRx and the baseline achieve a higher performance with just 1 pilot. The gain provided by EqDeepRx is again in the order of 2 dB, similar to what was observed under the non-line-of-sight scenario in CDL-C.

Finally, let us consider the achieved BLER under the UMa channel model, which is shown in Fig. 9. Now, the overall gain provided by EqDeepRx is somewhat higher than with the CDL channel models. Looking again at the BLER value of 10%, EqDeepRx yields a gain of more than 4 dB. One explanation for this is the fact that EqDeepRx was also trained with UMa channel data. Despite the random nature of this channel model, there are still opportunities for data-driven

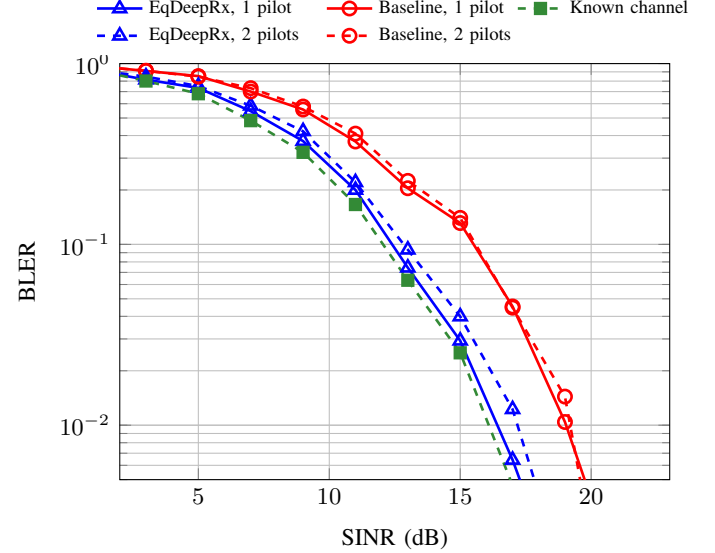


Fig. 8: BLER with CDL-D, UE speed of 10–15 m/s, and RMS delay spread of 10–100 ns.

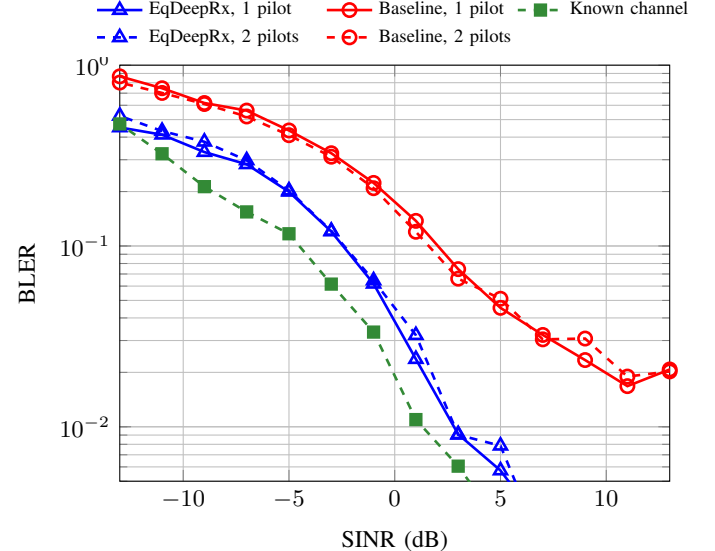


Fig. 9: BLER with UMa and UE speed of 10–15 m/s. Data rate matched MCSs.

receivers to optimize their behaviour for the prevailing data distribution. Moreover, similar to CDL-C, there is practically no difference in the performance of the receivers with 1 DMRS and 2 DMRSs, indicating that in this scenario the additional redundancy provided by the reduced overhead is comparable to a more accurate channel estimate.

Altogether, these validation results indicate robust performance of the EqDeepRx model. It can provide a substantial performance gain across all the evaluated channel conditions and models. The authors have also done several additional validation experiments, where similar performance was observed, although they have been omitted from this article for brevity.

### B. Spectral efficiency

To obtain a better understanding of the spectral efficiency improvement achievable by EqDeepRx, additional validations

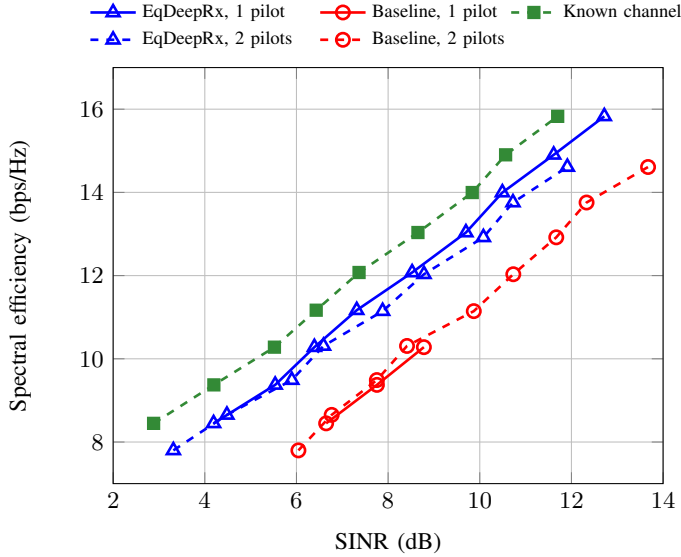


Fig. 10: Spectral efficiency, using CDL-C and UE speed of 10–15 m/s.

have been performed with a set of MCS values under CDL-C channel model, with UE speeds of 10–15 m/s. The SINR required to achieve a target BLER of 10% is measured by averaging over multiple channel realizations and SINR values. The achieved SINR values are then coupled with the corresponding spectral efficiency achievable with that particular MCS and DMRS configuration. This yields individual data points that can be plotted on an SINR vs. spectral efficiency plot. In particular, the spectral efficiency is defined as follows:

$$SE = N_T Q_m r (1 - \text{BLER}_{\text{target}}) \rho \gamma, \quad (14)$$

where  $N_T$  is the number of MIMO layers,  $Q_m$  is the number of bits per symbol (6 with 64-QAM),  $r$  is the code rate,  $\text{BLER}_{\text{target}}$  is the target BLER of 10%,  $\rho$  is the proportion of data-carrying REs (13/14 or 12/14 with 1 and 2 pilots, respectively), and  $\gamma$  is the proportion of the useful signal duration in the OFDM symbol ( $\gamma \approx 0.93$  in our simulation scenario). Note that when calculating the spectral efficiency, we use the target code rate as the value of  $r$  in (14), although the true proportion of information bits varies slightly due to rounding and padding. We observed these discrepancies to be within 1.5% under our simulation configurations, with typical discrepancies well below 1%. Therefore, the impact on the results is negligible.

The resulting spectral efficiencies are shown in Fig. 10, where the markers denote the specific SINR points in which the BLER target is achieved, while the line is the result of interpolation between these individual data points. If target BLER cannot be achieved with a certain MCS value, it is omitted from the figure. It can be observed that the performance of the EqDeepRx is consistently high across the whole SINR range, which covers the 64-QAM MCSs from index 11 through 19. Moreover, with the higher MCSs, it seems to be beneficial to use the 1 pilot configuration with EqDeepRx since it provides the highest spectral efficiency. The baseline is not able to benefit from the 1 pilot configuration since it requires 2 pilots in order to achieve the target BLER with MCSs above 13. Altogether, the

spectral efficiency gain of EqDeepRx over the baseline solution is approximately 15–25%, depending on the SINR level. This is essentially the throughput gain achievable by the proposed scheme.

### C. Model complexity and ablation studies

A key design decision for the developed EqDeepRx algorithm is the selection of the equalizer(s) that provides the soft symbol estimates for the subsequent ML processing. To understand better the impact of different equalization approaches on the final model performance, Fig. 11 shows the BLER for CDL-C validation under four different equalizer combinations. In addition to the adopted structure with parallel LMMSE and RZF equalizers, we also evaluated the performance with some combinations that included a matched filter (MF) type approach. This equalizer consists of a matched filter in spatial domain, which corresponds to an output of  $x_{ij, \text{MF}} = \hat{\mathbf{H}}_{ij} \mathbf{y}_{ij}$ .

From Fig. 11 it is evident that the combinations incorporating the LMMSE equalizer perform the best in terms of BLER. The option with LMMSE and RZF equalizers, corresponding to the primary EqDeepRx architecture, achieves the lowest BLER, while adding the MF equalizer has no impact on the performance. Utilizing LMMSE and MF equalizers has a slightly worse performance. Together, these observations indicate that the information provided by the MF is insufficient compared to the RZF output from the perspective of the subsequent ML processing. If removing the LMMSE equalizer and using only RZF and MF equalizers, the performance drops by approximately 5 dB due to inter-cell interference.

Additionally, we note that we could not train a functional model by utilizing solely the LMMSE equalizer with DenoiseNN included in the model. Our hypothesis for the instability is that, when DenoiseNN pre-processes input data with initial random weights, the LMMSE calculation especially with INCM estimation becomes numerically too unstable to proceed with optimization. When another EQ such as RZF is included, this alternative EQ can pass sufficient information for training of neural network components even at the initial stage when the neural network weights are near random. Figure 11 also includes options without DenoiseNN in which case also an LMMSE-only model can be trained. Nevertheless, the model employing both LMMSE and RZF is performing best also among models without DenoiseNN, although falling short of the corresponding model that incorporates DenoiseNN.

Next, let us evaluate EqDeepRx's capability of dealing with an arbitrary number of MIMO layers. This feature was tested by evaluating different EqDeepRx models with 2 and 4 layers. In particular, three different EqDeepRx models were trained with data consisting of 2 UEs, 4 UEs, and 2–4 UEs. Similar to the primary simulation assumptions, each UE has one transmit antenna, which means that the number of UEs directly translates to the number of overlapping MIMO layers.

The corresponding BLER results are shown in Fig. 12. Firstly, it is evident from the results that the EqDeepRx model generalizes well to different numbers of MIMO layers when the training data includes example of all options. This is evidenced by the fact that the model trained with 2–4 MIMO layers achieves identical performance with the models that have been

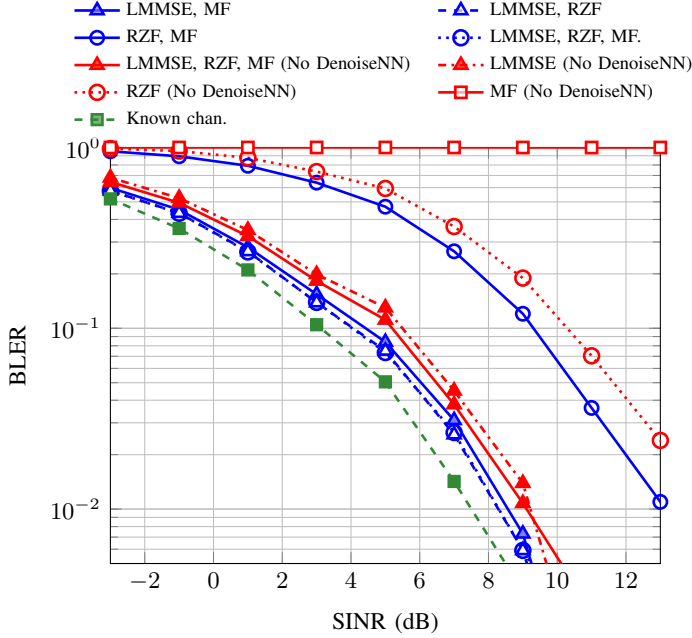


Fig. 11: Ablation study on the parallel equalizers in 1-pilot setup. CDL-C, speed 10–15 m/s.

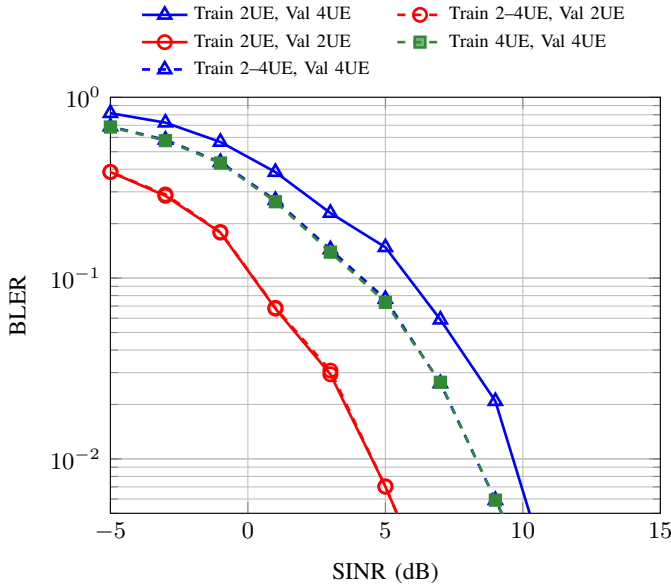


Fig. 12: MIMO layer count generalization (2 vs. 4 UEs) with 1-pilot setup. Train–valid mismatch is shown for comparison for 2 and 4 UEs. CDL-C, speed 10–15 m/s.

trained with the prevailing number of layers, in both cases of 2 and 4 UEs. The model that has been trained only with 2 UEs falls short of the generalized model when evaluated with 4 UEs. In this case, the performance deficit is approximately 1.5 dB. Therefore, it can be concluded that the EqDeepRx model can support different numbers of MIMO layers, as long as the training data set contains samples of all scenarios.

Then, to investigate the effect of model complexity on the BLER performance, we trained EqDeepRx models of different sizes and architectures and evaluated them with CDL-C channel, focusing on the 1 DMRS scenario. Two different

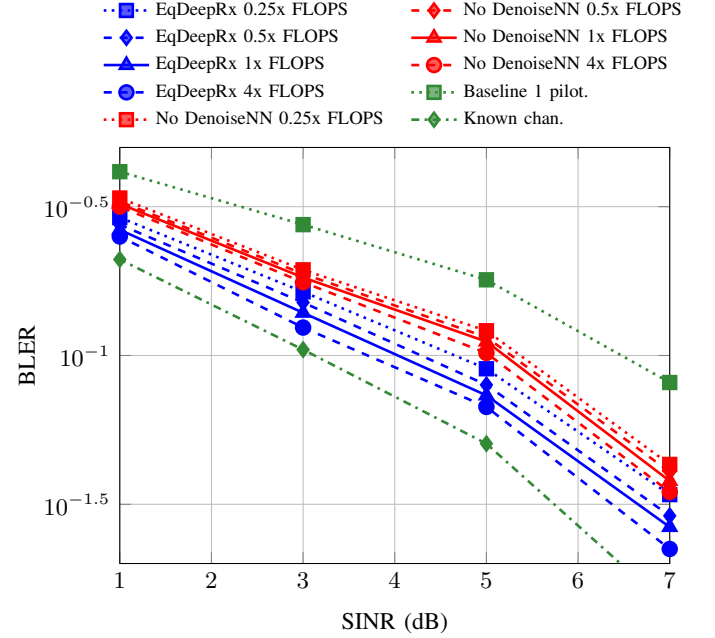


Fig. 13: Models with different FLOPS complexity in 1-pilot setup. CDL-C, speed 10–15 m/s.

architectures were considered: the full EqDeepRx model and a reduced EqDeepRx model without the DenoiseNN block. Both architectures were trained with four different model sizes, which are quantified in terms of number of FLOPS with respect to the primary EqDeepRx model architecture.

The results of this experiment are collected in Fig. 13. Firstly, it can be observed that none of the architectures without the DenoiseNN block can outperform the full EqDeepRx model, regardless of complexity. Even the model with four times higher complexity in the detector and demapper CNNs falls 0.2 dB short of the smallest EqDeepRx model that has 16 times fewer FLOPS. This indicates that it is crucial to allocate the ML processing to the right parts of the receiver, since that allows for achieving the best balance between complexity and performance. As for the EqDeepRx models, allocating more FLOPS to the model does seem to yield consistently higher performance. Quadrupling the FLOPS of the primary EqDeepRx architecture provides a gain of 0.2–0.3 dB in terms of BLER, at least in this particular scenario. However, we wish to emphasize that the exact amount of gain most likely depends on the adopted simulation scenario, especially the MCS. Nevertheless, these observations demonstrate that the proposed EqDeepRx receiver can be flexibly optimized for the desired performance and complexity targets, which depend on the available hardware, power, and throughput requirements. Such flexible optimization might not be possible with conventional non-ML receivers.

We also evaluated an entirely different alternative model architecture, which consists of a monolithic detector and demapper, as opposed to EqDeepRx that relies on per-layer detector and demapper CNN models. The drawback of such a monolithic approach is that it cannot generalize to different numbers of MIMO layers, unlike EqDeepRx. Figure 14 shows the performance of the monolithic approach along with the

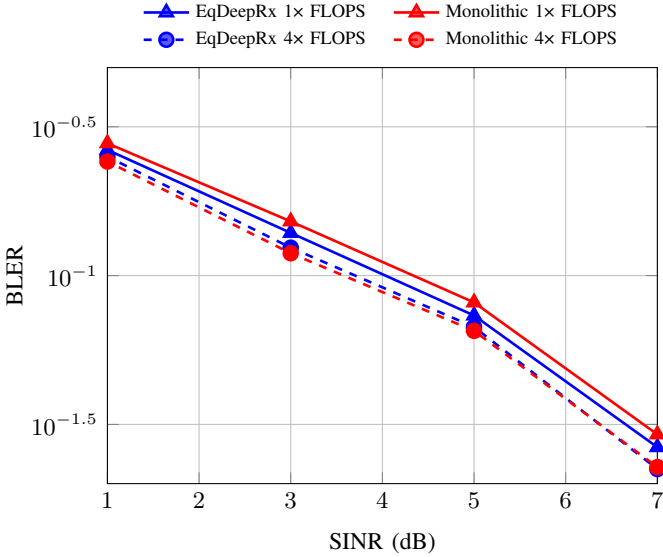


Fig. 14: EqDeepRx vs Monolithic detector and demapper. All options include DenoiseNN and LMMSE and RZF equalization. CDL-C, speed 10–15 m/s.

Model	GFLOPs			Params (k)	SINR@ 10%BLER
	Denoise	Detec	Demap		
EqDeepRx 0.25x	0.02	0.06	0.02	0.10	29
EqDeepRx 0.5x	0.03	0.10	0.05	0.18	55
EqDeepRx 1x	0.05	0.26	0.06	0.37	116
EqDeepRx 4x	0.16	1.07	0.21	1.44	472
NoDenoise 0.25x	–	0.08	0.02	0.10	26
NoDenoise 0.5x	–	0.14	0.05	0.19	49
NoDenoise 1x	–	0.30	0.06	0.37	104
NoDenoise 4x	–	1.21	0.24	1.45	427
Monolithic 0.25x	0.01	0.05	0.04	0.10	96
Monolithic 0.5x	0.02	0.10	0.05	0.18	176
Monolithic 1x	0.03	0.18	0.15	0.36	346
Monolithic 4x	0.05	1.20	0.23	1.48	1751
No LMMSE 1x	0.05	0.26	0.06	0.37	116
No LMMSE 4x	0.16	1.07	0.21	1.44	472
					9.35

TABLE III: Per-part and total GFLOPs per inference per 16 PRB (192 subcarriers) / 1 MIMO layer. Also parameter counts (equalizers excluded) and performance are shown.

EqDeepRx model with two different model sizes, aligned in terms of FLOPS. With the smaller model, EqDeepRx slightly outperforms the monolithic model, despite its more restricted nature. With the quadrupled model complexity, the performance of the two models is nearly aligned. These findings indicate that the approach adopted in EqDeepRx does not sacrifice performance in order to achieve MIMO layer independence.

The findings and details regarding the complexity and performance of all the different ML receiver model variants are collected in Table III. It lists the FLOPS per inference for each ML block, as well as the number of trainable parameters. Note that the non-ML receiver elements are not considered in the table, since the focus is on the additional complexity of the ML processing. Table III also shows the SINR required to achieve the target BLER of 10% in the considered simulation scenario (CDL-C, UE speed of 10–15 m/s, 1 DMRS, MCS 11). The primary EqDeepRx architecture has an additional complexity of 0.37 GFLOPs per inference, with most of the complexity residing in the DetectorNN block. The most complex architecture evaluated is the monolithic 4x model with

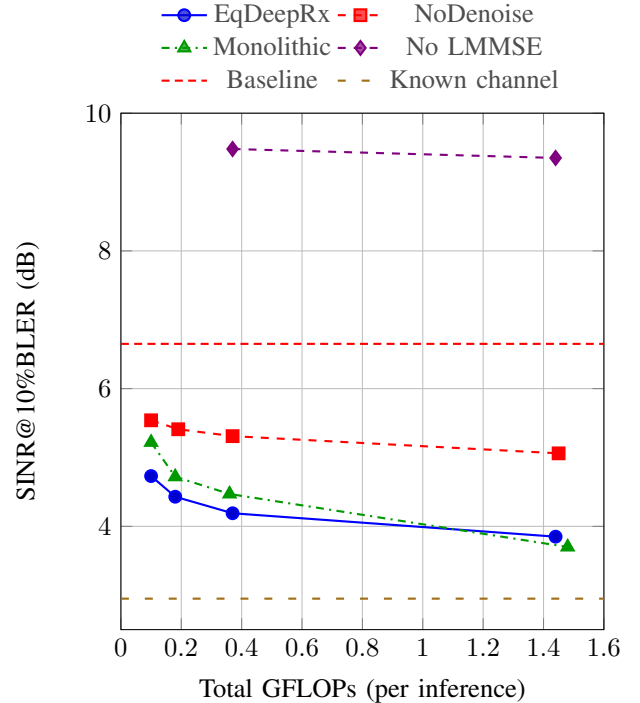


Fig. 15: SINR vs. total compute across DeepRx model families and hyperparameter variants. Baseline is the performance of the non-learned LMMSE baseline. Each dot represents a trained model with different hyperparameters. CDL-C, speed 10–15 m/s.

a complexity of 1.48 GFLOPs per inference, and it is able to outperform the primary EqDeepRx approach by only 0.5 dB. This indicates the proposed EqDeepRx model demonstrates a rather favorable balance between performance and complexity.

Finally, to further evaluate the performance–complexity trade-off of the considered augmented receiver models, Fig. 15 visualizes the SINR and FLOPs results of Table III. It can be observed that the proposed EqDeepRx model achieves the highest performance in the lower FLOPs regime, while the monolithic approach slightly outperforms it under higher complexity. Moreover, it can be seen that the effect of the additional DenoiseNN is approximately 1 dB, regardless of the model complexity. The model variant without LMMSE equalizer falls clearly short of all other options, regardless of the number of FLOPs. Altogether, the shape of the curves indicates that additional complexity yields diminishing returns when the model size is increased. With EqDeepRx, we have aimed at operating in the regime where the model complexity has a clear impact on the receiver performance.

## V. CONCLUSION

This article presented *EqDeepRx*, a practical ML-aided MIMO OFDM receiver that combines expert signal processing with compact neural components to deliver high link performance at low complexity. The design (i) denoises DMRS-based channel estimates with a lightweight DenoiseNN, (ii) runs two complementary linear equalizers (LMMSE and RZF) in parallel to avoid learning matrix inverses, and (iii) performs per-MIMO-layer data-aided detection and demapping with shared weights,

enabling near-linear complexity growth with layer count and layer-count invariance. Building on earlier DeepRx insights, all variants observe the full time-frequency OFDM grid and allow DetectorNN to learn a data-aided detection scheme.

Extensive simulations with 5G/6G-compliant OFDM and LDPC coding show consistent improvements over a strong conventional baseline. Across CDL-C, CDL-D, and UMa channel models, *EqDeepRx* reduces the SINR at 10% BLER by about 2 dB (CDL-C) and by more than 4 dB (UMa), and improves spectral efficiency by roughly 15–25%. It maintains comparable BLER with one or two DMRS symbols and remains robust up to 30–35 m/s; in contrast, the baseline struggles with one DMRS under high mobility.

Ablation studies show that (a) the LMMSE+RZF equalizer pair is essential, adding MF brings no benefit, and removing interference-handling LMMSE degrades performance by up to 5 dB; (b) DenoiseNN is critical; omitting it costs 1 dB even with a larger detector/demapper; and (c) per-layer detection/demapping matches or exceeds monolithic designs while uniquely supporting arbitrary MIMO layer counts.

In summary, *EqDeepRx* delivers robust BLER and throughput gains over a conventional receiver while preserving low computational complexity and deployment practicality. By keeping classical estimation and equalization in the loop and focusing learning capacity where it has the highest payoff (channel denoising and data-aided detection), *EqDeepRx* avoids emulating matrix inverses and remains resilient under interference, mobility, and channel variability.

As future work, we will investigate reducing DMRS density and handling RF-chain nonlinearities (e.g., PA saturation, IQ imbalance, quantization) within *EqDeepRx*.

## REFERENCES

- [1] T. O’Shea and J. Hoydis, “An Introduction to Deep Learning for the Physical Layer,” *IEEE Transactions on Cognitive Communications and Networking*, vol. 3, no. 4, pp. 563–575, Dec. 2017.
- [2] H. He, S. Jin, C.-K. Wen, F. Gao, G. Y. Li, and Z. Xu, “Model-Driven Deep Learning for Physical Layer Communications,” *IEEE Wireless Communications*, vol. 26, no. 5, pp. 77–83, Oct. 2019.
- [3] H. Huang, S. Guo, G. Gui, Z. Yang, J. Zhang, H. Sari, and F. Adachi, “Deep Learning for Physical-Layer 5G Wireless Techniques: Opportunities, Challenges and Solutions,” *IEEE Wireless Communications*, vol. 27, no. 1, pp. 214–222, Feb. 2020.
- [4] M. Honkala, D. Korpi, and J. M. J. Huttunen, “DeepRx: Fully Convolutional Deep Learning Receiver,” *IEEE Transactions on Wireless Communications*, vol. 20, no. 6, pp. 3925–3940, Jun. 2021.
- [5] D. Korpi, M. Honkala, J. M. Huttunen, and V. Starck, “DeepRx MIMO: Convolutional MIMO Detection with Learned Multiplicative Transformations,” in *ICC 2021 - IEEE International Conference on Communications*, Jun. 2021, pp. 1–7.
- [6] D. Neumann, T. Wiese, and W. Utschick, “Learning the MMSE Channel Estimator,” *IEEE Transactions on Signal Processing*, vol. 66, no. 11, pp. 2905–2917, Jun. 2018.
- [7] H. He, C.-K. Wen, S. Jin, and G. Y. Li, “Deep Learning-Based Channel Estimation for Beamspace mmWave Massive MIMO Systems,” *IEEE Wireless Communications Letters*, vol. 7, no. 5, pp. 852–855, Oct. 2018.
- [8] Z. Qin, H. Ye, G. Y. Li, and B.-H. F. Juang, “Deep Learning in Physical Layer Communications,” *IEEE Wireless Communications*, vol. 26, no. 2, pp. 93–99, Apr. 2019.
- [9] Z. Zhao, M. C. Vuran, F. Guo, and S. D. Scott, “Deep-Waveform: A Learned OFDM Receiver Based on Deep Complex-Valued Convolutional Networks,” *IEEE Journal on Selected Areas in Communications*, vol. 39, no. 8, pp. 2407–2420, Aug. 2021.
- [10] H. Kim, S. Oh, and P. Viswanath, “Physical Layer Communication via Deep Learning,” *IEEE Journal on Selected Areas in Information Theory*, vol. 1, no. 1, pp. 5–18, May 2020.
- [11] H. Ye, G. Y. Li, and B.-H. Juang, “Power of Deep Learning for Channel Estimation and Signal Detection in OFDM Systems,” *IEEE Wireless Communications Letters*, vol. 7, no. 1, pp. 114–117, Feb. 2018.
- [12] X. Gao, S. Jin, C.-K. Wen, and G. Y. Li, “ComNet: Combination of Deep Learning and Expert Knowledge in OFDM Receivers,” *IEEE Communications Letters*, vol. 22, no. 12, pp. 2627–2630, Dec. 2018.
- [13] N. Samuel, T. Diskin, and A. Wiesel, “Learning to Detect,” *IEEE Transactions on Signal Processing*, vol. 67, no. 10, pp. 2554–2564, May 2019.
- [14] S. Cammerer, F. A. Aoudia, J. Hoydis, A. Oeldemann, A. Roessler, T. Mayer, and A. Keller, “A Neural Receiver for 5G NR Multi-User MIMO,” in *2023 IEEE Globecom Workshops (GC Wkshps)*, Dec. 2023, pp. 329–334.
- [15] J. Clausius, M. Rübenacke, D. Tandler, and S. ten Brink, “Joint Detection and Decoding: A Graph Neural Network Approach,” *IEEE Transactions on Communications*, vol. 73, no. 10, pp. 9043–9058, Oct. 2025.
- [16] S. Norouzi, M. Rahmani, Y. Chu, T. Braun, K. Chowdhury, and A. Burr, “Lightweight Graph Neural Networks for Enhanced 5G NR Channel Estimation,” in *2025 IEEE 36th International Symposium on Personal, Indoor and Mobile Radio Communications (PIMRC)*, Sep. 2025, pp. 1–7.
- [17] Z. Liu, N. Wu, D. He, W. Yuan, Y. Li, and T. Q. S. Quek, “GNN-Assisted BiG-AMP: Joint Channel Estimation and Data Detection for Massive MIMO Receiver,” *IEEE Transactions on Wireless Communications*, vol. 24, no. 6, pp. 4631–4646, Jun. 2025.
- [18] J. Pihlajasalo, D. Korpi, M. Honkala, J. M. J. Huttunen, T. Riihonen, J. Talvitie, A. Brihuega, M. A. Uusitalo, and M. Valkama, “Deep Learning OFDM Receivers for Improved Power Efficiency and Coverage,” *IEEE Transactions on Wireless Communications*, vol. 22, no. 8, pp. 5518–5535, Aug. 2023.
- [19] H. Farhadi, J. Haraldson, and M. Sundberg, “A Deep Learning Receiver for Non-Linear Transmitter,” *IEEE Access*, vol. 11, pp. 2796–2803, 2023.
- [20] S. Cammerer, F. A. Aoudia, S. Dörner, M. Stark, J. Hoydis, and S. ten Brink, “Trainable Communication Systems: Concepts and Prototype,” *IEEE Transactions on Communications*, vol. 68, no. 9, pp. 5489–5503, Sep. 2020.
- [21] D. Korpi, M. Honkala, and J. M. Huttunen, “Deep Learning-Based Pilotless Spatial Multiplexing,” in *2023 57th Asilomar Conference on Signals, Systems, and Computers*, Oct. 2023, pp. 1025–1029.
- [22] C. K. Lo, F. Carpi, J. Cho, and C. J. Zhang, “AI/ML-Based Asymmetric Modulation Constellations and Pilotless Communications,” in *2025 IEEE 101st Vehicular Technology Conference (VTC2025-Spring)*, Jun. 2025, pp. 1–5.
- [23] J. Cheng, W. Chen, and B. Ai, “Adaptive End-to-End Transceiver Design for NextG Pilot-Free and CP-Free Wireless Systems,” *IEEE Journal on Selected Areas in Communications*, pp. 1–1, 2025.
- [24] J. Zou, J. Xiao, Q. Mao, S. Liu, B. Xiao, and Y. Liang, “Deep Receiver for Multi-Layer Data Transmission with Superimposed Pilots,” in *ICASSP 2025 - 2025 IEEE International Conference on Acoustics, Speech and Signal Processing (ICASSP)*, Apr. 2025, pp. 1–5.
- [25] E. Raninen, “Oracle Approximating Shrinkage Covariance Matrix Estimators for Complex Elliptical Distributions,” in *2024 32nd European Signal Processing Conference (EUSIPCO)*, Aug. 2024, pp. 2717–2721.
- [26] Y. Chen, A. Wiesel, Y. C. Eldar, and A. O. Hero, “Shrinkage Algorithms for MMSE Covariance Estimation,” *IEEE Transactions on Signal Processing*, vol. 58, no. 10, pp. 5016–5029, Oct. 2010.
- [27] D. Hui, S. Sandberg, Y. Blankenship, M. Andersson, and L. Grosjean, “Channel Coding in 5G New Radio: A Tutorial Overview and Performance Comparison with 4G LTE,” *IEEE Vehicular Technology Magazine*, vol. 13, no. 4, pp. 60–69, Dec. 2018.
- [28] R. Liu, J. Lehman, P. Molino, F. Petroski Such, E. Frank, A. Sergeev, and J. Yosinski, “An intriguing failing of convolutional neural networks and the CoordConv solution,” in *Advances in Neural Information Processing Systems*, vol. 31. Curran Associates, Inc., 2018.
- [29] J. Peng, L. Xie, Z. Zhang, T. Tan, and J. Wang, “Accelerating Deep Neural Networks with Spatial Bottleneck Modules,” Sep. 2018.
- [30] J. Jin, A. Dundar, and E. Culurciello, “Flattened Convolutional Neural Networks for Feedforward Acceleration,” Nov. 2015.
- [31] E. Littwin and L. Wolf, “Regularizing by the Variance of the Activations’ Sample-Variances,” in *Advances in Neural Information Processing Systems*, vol. 31. Curran Associates, Inc., 2018.
- [32] J. Hoydis, S. Cammerer, F. A. Aoudia, A. Vem, N. Binder, G. Marcus, and A. Keller, “Sionna: An Open-Source Library for Next-Generation Physical Layer Research,” Mar. 2023.
- [33] 3GPP TR 38.901, “Study on channel model for frequencies from 0.5 to 100 GHz,” Dec. 2025.
- [34] 3GPP TS 38.214, “Physical layer procedures for data,” Dec. 2025.